

LDV MEASUREMENTS OF THE VELOCITY FIELD WITHIN A RIBBED INTERNAL DUCT FLOW

EDWARD HUCKLE
MAE DEPT. UCLA

DEJAN PANTELIC
TECHNICAL UNIVERSITY OF MUNICH

KUNZHONG HU
MAE DEPT. UCLA

STANLEY JONES
MAE DEPT. UCLA

VLADIMIR TRAVKIN
MAE DEPT. UCLA

IVAN CATTON
MAE DEPT. UCLA

KEYWORDS: *LDV, TURBULENCE, CHANNEL WALL ROUGHNESS*

ABSTRACT

Laser Doppler velocimetry (LDV) has been used to measure the velocity field in an internal duct flow of air with regular rib roughness. The experiments were conducted to study the effect regular wall obstacles have on the flow velocity field. The instantaneous u and v velocities were measured in both a smooth and rough rectangular duct. For the smooth channel the wind tunnel Reynolds number capability was first investigated and was shown to be linear with blower shaft frequency, having a range of 13000 - 42000. Next, the turbulent velocity profiles were measured in the smooth channel for 6 different blower speeds (Reynolds numbers), and the results greatly resembled those found in previous literature.

Twenty sets of rectangular, 6.35 mm x 6.35 mm ribs were then mounted to the top and bottom of the channel with a spacing of 75 mm ($P/H = 11.8$). A grid of nodes were selected and the turbulent velocities were measured for a given Reynolds number, and are presented and discussed. Valuable insight was gained which will aid in future studies intended to measure the Reynolds stress and other closure terms.

NOMENCLATURE

a	= 50 mm, duct height
b	= 150 mm, duct width
d	probe volume size
D_H	hydraulic diameter
f	frequency
H	rib height
M	vector/array magnitude
P	rib pitch
r	radius
Re	Reynolds number

S/N	signal to noise ratio
t	time
$u, (U)$	instantaneous (mean) velocity in x-direction
u'	velocity fluctuation in the x-direction
$v, (V)$	instantaneous (mean) velocity in y-direction
v'	velocity fluctuation in the y-direction
y^*	$= y / (a/2)$

Greek Symbols

*	fringe size/spacing
ω	angular frequency

INTRODUCTION

To enhance the heat transfer on a surface repeated ribs are frequently used. The ribs disrupt the laminar sublayer and create local wall turbulence due to flow separation and reattachment between the ribs, which greatly enhances the heat transfer. This phenomenon has been of great interest for the past 20 years because of its wide range of engineering application. Many researchers have contributed in the experimental study of flow and heat transfer in rib roughened ducts such as Olsson and Sunden (1998), Hwang and Liou (1994 and 1995), Liou et al. (1990), Liou et al. (1995), Zhang et al. (1995), and Han (1988). As mentioned in Naimi & Gessner (1997), "Previous research on flow in rectangular ducts with periodically spaced ribs has focused primarily on two aspects of the overall problem, namely: (1) understanding the nature of local flow and heat transfer in the entire duct cross section midway between, and directly above, adjacent ribs, and (2) understanding the nature of local flow and heat transfer in the duct mid-plane region, with specific emphasis on Nusselt number behavior along the rib-roughened surface and the sensitivity of this behavior to rib geometry, spacing, offset distance from the

wall, etc." Considerable data have been reported for rib roughened heat transfer and pressure drop in the flow over rough ribs for internal duct flow.

Although substantial work has been done for the study of duct flow, the experimental studies on turbulent flow past multiple pairs of ribs on two sides of a duct are still in its infancy, especially study of the turbulent kinetic energy distribution along the duct is lacking. Additionally, the influence of the rib pitch on the flow characteristics needs to be investigated. Outstanding work in this field can be found in Rosen and Tragardh (1994), which measured the $\langle u'v' \rangle$ correlation in the near wall region over a wide range of Reynolds numbers by LDV. Liou et al. (1990) characterized the turbulent flow past two pairs of ribs arranged on opposite sides of a rectangular duct for various Reynolds numbers and pitches through LDV technique. So, one objective of this study was to measure the fluctuation velocity and turbulent kinetic energy across the duct with rib roughened walls.

Another objective of this study was to contribute to the development of a closure model for incompressible flow in a rough channel. A one dimensional flow model for fully developed steady state conditions that accounts for the morphological structure of the rough wall layer was developed by Travkin and Catton (1992, 1995). The data generated from this study can serve as a foundation upon which future closure modeling efforts may lie.

EXPERIMENTAL FLOW APPARATUS

The flow generation apparatus consisted of a blower to power the flow, a particle feeder, a flow conditioning section, the test section, and a particle recoverer. The flow system was an open loop for the air but it was a closed loop for the seeding particles (because the seeding particles were recovered). A centrifugal blower was used and was powered by a 1 hp variable speed motor. The blower shaft frequency was controlled by a speed controller.

The dimensions of the particle feeder/recovery box were 0.340 x 0.280 x 0.340 m. Its function was to house the seeding particles inside a box and regulate the circulation of particles through the open loop wind tunnel. On the top of the box was a HEPA filter serving the dual purpose of recovering the seed particles for reuse and ensuring that they did not escape into the laboratory environment.

The test section duct was made of 6.35 mm plexiglass, had the length of 1500 mm and a cross section of 150 mm (depth) x 50 mm (height). For the rough channel measurements twenty ribs were glued regularly arranged (spaced every 75 mm) on opposite sides (top and bottom) of the duct. The ribs were made of plexiglass square rods of cross-section size 6.35 mm x 6.35 mm. To ensure fully developed flow in the test section, an entrance duct was constructed preceding the test section. The entrance duct was 1500 mm long and had a rectangular cross section 150 mm (depth) x 50 mm (height). Additionally a screen and honeycomb flow straighteners were added into the channel to ensure fully developed flow for the test section.

OPTICAL & ELECTRONIC TECHNIQUE AND APPARATUSES

Laser Technique (LDV)

Two component heterodyne laser Doppler velocimetry (LDV) was used to measure the u (x - direction) and v (y -direction) components of instantaneous velocity. The light source used was a Spectra Physics model 165 argon-ion laser. The multi-line mode for the laser was used resulting in several superposed beams in the blue-green range. An equilateral prism was used to separate all of the beams and the two strongest beams - green ($\lambda = 514.5$ nm) and blue ($\lambda = 488$ nm) were selected, accomplished by optically truncating the undesired beams. The green light was chosen to construct the vertically oriented LDV fringe pattern (for measuring the u component of velocity) while the blue light was chosen to measure the v component (horizontally oriented).

The beams were then individually split (maintaining polarization) using cube beamsplitters. From this stage the green beams, spaced 25 mm, were focused into the probe volume using a 180 mm focal length transmitter lens. This led to a probe volume size of 60 microns, with 16 fringes 3.70 microns in size (δ_{green}). Similarly, for the blue beams, the beam spacing was 30 mm giving a probe volume of 56 microns and 19 fringes of 2.93 micron size (δ_{blue}). Both fringe patterns were superposed to constitute one probe volume capable of measuring u and v . To generate direction sensitivity in the v velocity component Isomet model 1201-E acusto-optic modulators with 221A-2 drivers were used to amplitude modulate the blue beams. These modulators had a center frequency of 40 MHz. The two drivers drove the modulators at 40 MHz & 43 MHz creating a 3 MHz shift.

The receiver configuration used was backscatter using the transmitter lens for scattered light collimation. The scattered light was directed into a fiber-optic patchcord and into a photo-multiplier tube driven by a C6270-DP socket. Alignment was assisted and verified using a small wire mounted on a rotating wheel. Using the v -component, the velocity calculated by $v = r_{\text{wheel}} \omega$ and calculated from LDV differed by only 0.6 %.

Electronic Signal Capturing

The electronic signal was first amplified with a Stanford Systems model SR445 pre-amplifier. and then digitized using a Gage Compuscope 265 A/D card. LabVIEW 4.1 Full Development Studio was used both for A/D card hardware control and also for the signal processing needs. Chronologically, an entrained particle crossing the probe volume would create an optical light burst leading to an analog electronic signal. When the voltage of one of the electronic "bursts" exceeded the threshold voltage a trigger event would occur and a specified number of points would then be designated as the burst signal. After each trigger event LabVIEW would transfer the burst signal to the LDV analysis software VI (virtual instrument) for processing.

LDV Signal Analysis

The raw digitized signal was displayed for visual user verification of burst quality. The signal was next filtered using an equi-ripple high-pass filter for signal pedestal removal (always present in LDV signals). A digital power spectrum was then performed on the filtered signal in order to determine the burst frequency, f_b , proportional to the velocity by $u = f_b \delta$. In order to mathematically quantify the quality of each burst a signal to noise criteria was developed, and is given by:

$$S/N = \frac{M_{\text{signal}}}{M_{\text{noise}}} \quad (1)$$

For this relation, M corresponding to the magnitude of a vector array (evaluated using an inner product). The power spectrum of an LDV signal is a delta function at the burst frequency. Thus, M_{signal} was the magnitude of the sub-array surrounding the delta function and M_{noise} is the magnitude of the remaining power spectrum array. Signals of excellent quality (greatly resembling a delta function) would have a very high S/N (at least 10 or 100) whereas poor signals would have a S/N of less than unity. This enabled post filtering based on a minimum S/N criteria. The data was also manually post filtered to exclude the small occurrences of signals with high S/N but unrealistic frequencies (caused by multiple particles in the probe volume or other spurious signals). For each data point a statistically significant number of samples were taken (each consisting of a burst frequency realization and burst S/N) and statistical information was calculated.

EXPERIMENTAL RESULTS

The experimental results are illustrated as follows. The air tunnel Reynolds number capability was first evaluated. Then, experiments were performed which yielded results characterizing the velocity fields for both the smooth and the rough channel.

Air Tunnel Reynolds Number Capability

Before starting with the measurements for the smooth and the rough channel it was necessary to determine the achievable air tunnel Reynolds number capability. This is required in order to have a reference to other publications as well as to determine the turbulence range the measurements are going to be taken. Therefore the achievable Reynolds numbers were evaluated for the smooth channel. The measurements were taken in the center of the duct, since there can be found the maximum of the velocity profile. By utilizing the entire blower controller frequency range the duct center velocity vs blower frequency data was obtained. The Reynolds number is given by:

$$Re = \frac{U \cdot D_H}{\nu} \quad (2)$$

The duct hydraulic diameter D_H was evaluated as:

$$D_H = \frac{4ab}{2(a+b)} = 75 \text{ mm} \quad (3)$$

Hence, one gets a comparison between the blower controller frequency and the channel Reynolds number. These values are shown in Figure 1.

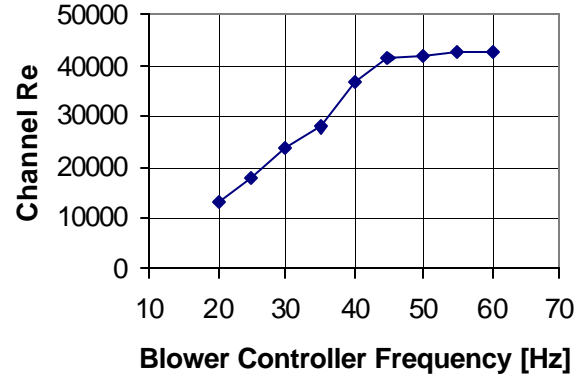


Figure 1 Air tunnel Reynolds number range

As shown in Figure 1 the lowest blower controller frequency to be used is 20 Hz. For lower frequencies the blower showed operating irregularities and are not useful. For blower frequencies between 20 Hz - 45 Hz the Reynolds number increases uniformly. After that the graph flattens and there is no significant increase of the Reynolds numbers. Even if we increase the blower controller frequency over 45 Hz no difference in the Reynolds number is achievable. That means a blower controller frequency range of 20 Hz - 45 Hz would be used. The Re-range evaluated was between 13000 - 42000.

Smooth Channel

Before constructing the rib-roughened channel it was first desired to measure the velocity profiles in the smooth rectangular channel, illustrating the quality of the flow.

For the smooth channel the mean as well as the fluctuation velocities in the x and y direction were evaluated. The results were all nondimensionalized by dividing by the reference velocity $U_{\text{Ref}} = 5.653 \text{ m/s}$. U_{ref} is the maximum velocity measured in the center of the duct for a blower controller frequency of 35 Hz.

Figure 2 shows the variation of the mean velocities over the height of the tunnel. It is seen to be typical of turbulent velocity profiles with a steep increase near the wall and a fairly uniform velocity near center line. In the immediate neighborhood of the wall no measurements could have been taken due to limitations in the access of LDV optics. As one can see in Figure 2 the few points measured near the wall exhibit the typical character in the boundary layer. Figure 2 also shows that for higher Reynolds numbers the curves in the boundary layer seem to be steeper. That means the boundary layer thickness decreases for higher Reynolds numbers. The effect of viscosity is smaller than that of inertia for larger Reynolds numbers.

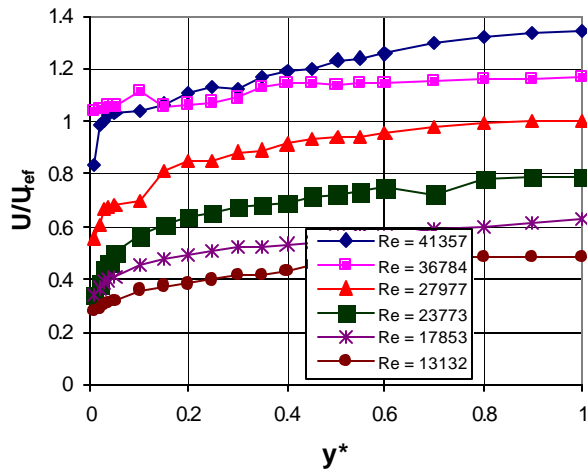


Figure 2 Nondimensional mean u-velocity profile

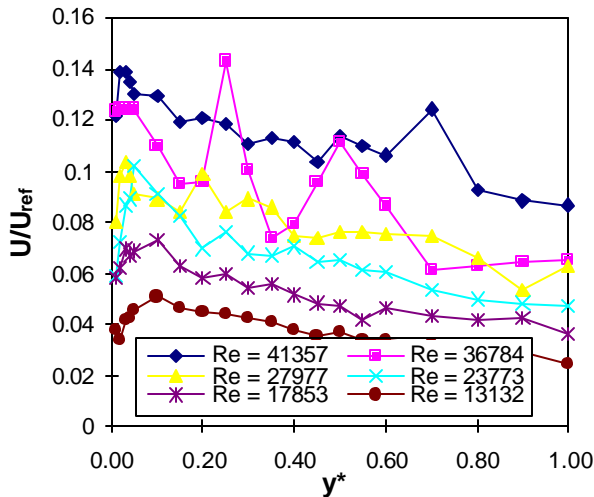


Figure 3 Nondimensional u-velocity fluctuation profile

In Figure 3 the longitudinal fluctuations over the height of the test section duct for different Reynolds numbers are illustrated. As one can see the curves exhibit a pronounced steep gradient and maximum close to the wall. These maxima are in the boundary layer. They seem to occur after the transitional layer. In this transitional layer the velocity fluctuations are very high and give rise to viscous stresses. Even closer to the wall the curves decrease to zero. At larger distances from the wall the velocities illustrate a continually decreasing behavior.

The mean velocities in the y -direction over the height of the channel are illustrated in Figure 4. These experiments were carried out to check the functionality of the Bragg Cells as well as to get a reference. The velocities are, as expected, close to zero since there should be no motion in the y -direction. Interesting though is that all velocities are showing positive values, which would indicate a net positive motion of particles towards the upper channel surface.

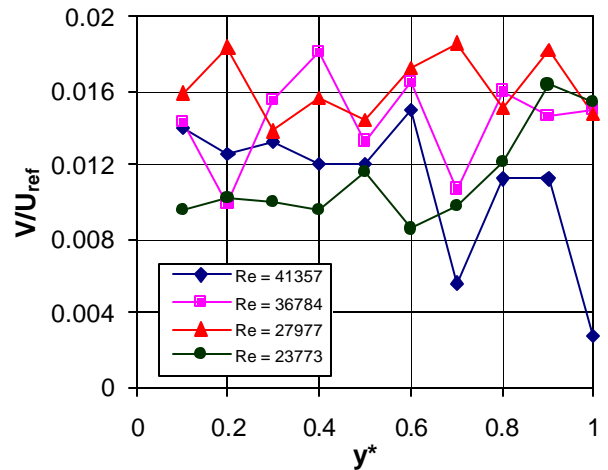


Figure 4 Nondimensional mean v-velocity profile

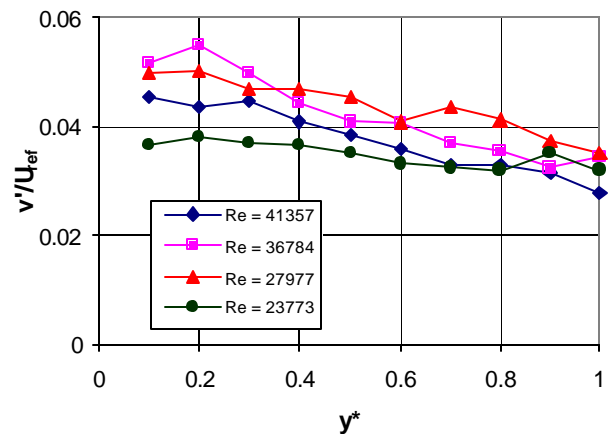


Figure 5 Nondimensional v-velocity fluctuation profile

Figure 5 shows the transverse fluctuation in the y -direction over the height of the channel. The profile is decreasing in the direction of the centerline. This is reasonable since the fluctuations are decreasing in direction of the centerline. The curves are supposed to have their maximum in the transitional layer and decrease to the wall to zero as can be seen in Schlichting (1960). In these measurements it was not possible to take any data in this region due to limited access for the LDV optics.

Rough Channel

For the ribbed channel a rib geometry was established and constructed and the instantaneous velocities were measured. The measurements were made for a speed controller frequency of 35 Hz. Figure 6 shows the measurement node locations.

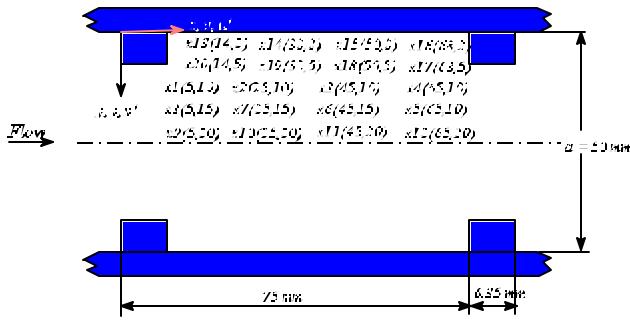


Figure 6 Locations of measurement node-points

As can be seen in Figure 6, each numbered node location is shown with corresponding coordinates (i.e. node 18 is at coordinates 50 mm in the x-direction and 5 mm in the y-direction). In Figure 7 the mean velocity over the height of the channel for different x positions are presented.

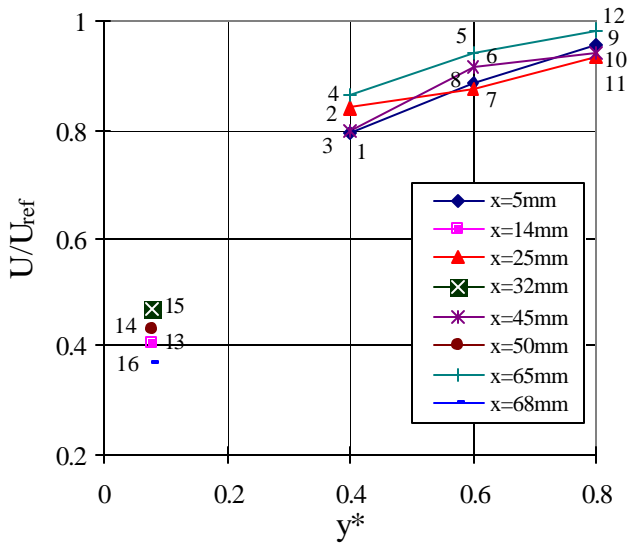


Figure 7 Mean u-velocities in rough channel

As one can see the velocity rises with the distance from the wall. This is plausible since the ribs hinder the flow near the wall. Since for the u component velocity measurements no Bragg Cells were used in order to achieve velocity direction sensitivity it is not possible to make any conclusions about the exact motion of the flow (mostly for nodes 13-20). Only the velocity values can be compared. For the flow direction just assumptions can be made.

By comparing the results from Figure 7 with the results gained for the smooth channel at speed controller frequency 35 [Hz], as seen in Figure 2, one can see that towards the centerline the velocity values for the rough and the smooth channel do not differ substantially. That means that close to the centerline there is no influence of the roughness elements evident any more. The flow profile approaches that of the fully developed duct flow.

The velocities for the points 13, 14, 15 and 16 (see Figure 6) indicate smaller values due to the fact that they are in the boundary layer where viscous forces are slowing down the flow.

Additionally, the flow is affected through the obstacle so that the velocities compared to the obtained results for the smooth channel are lower.

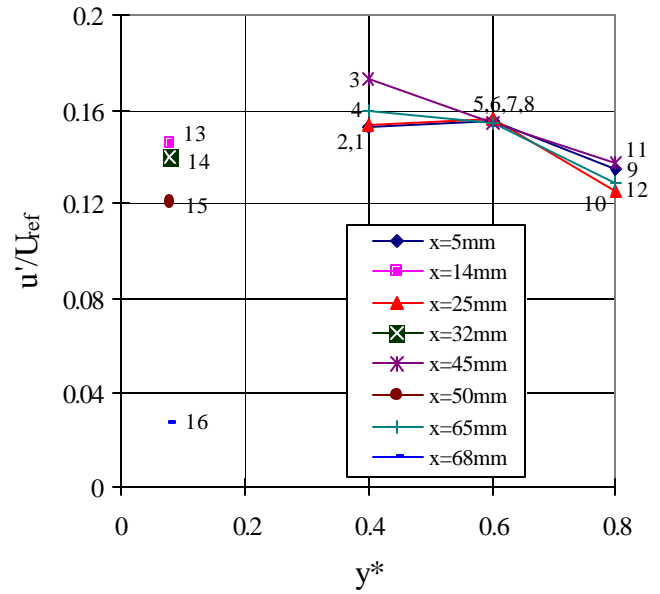


Figure 8 Fluctuation u-velocities in rough channel

In Figure 8 the fluctuation velocities in the rough channel for the measured grid points are shown. The profiles show that the highest fluctuations can be found over the rib height. Towards the centerline the fluctuations are decreasing.

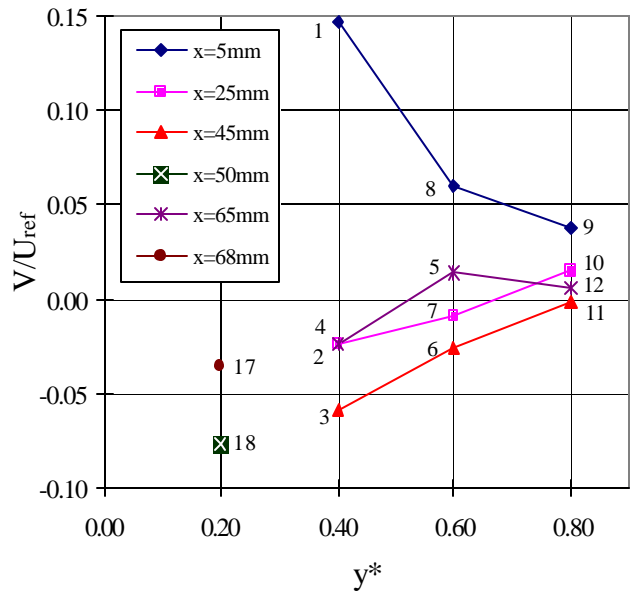


Figure 9 Mean v-velocities in rough channel

In Figure 9 the mean v-velocities for the rough channel are illustrated. Bragg Cells were used in order to achieve v-velocity direction sensitivity. Therefore, one can distinguish between negative and positive velocity directions and take more conclusions from the gained results.

As previously mentioned, flow over the rough surface can be separated into several main flow regions. The flow separates at the top of the first rib pair and forms a wake bubble. Afterwards it is assumed that the flow has enough time for reattachment. After starting redeveloping again there is another smaller separation bubble in front of the second rib.

Inspecting just the points for $x = 65 \text{ mm}$, see Figures 9 and 6, one can see that the experiments are showing that for point 4 the velocity shows in negative y direction. This is reasonable since after the rib the flow separates and then starts immediately with the reattachment. As one can see in Figure 6 the position of point 4 is already quite upstream. This is the reason why the velocity in the y -direction is not that high, since here the flow just started with the reattachment. Point 5 shows a small velocity in positive y direction. This point is farther away from the wall so that the reattachment starts earlier, since the ribs don't have a big effect there. The flow is for that distance just slightly turned away, but attaches earlier than the flow closer to the rib. This velocity should actually be near zero. For point 12 the flow profile approaches that of the fully developed duct flow and the velocity in the y -direction is almost zero.

If we take a look at the curve for $x = 45\text{mm}$ one can see that point 3 seems to be in the reattachment area, since the velocity points to the wall. Therefore we can also assume that below point 3 the separation bubble is active. Considering the distance to the next rib and comparing with other literature we can also assume that the flow will have enough time to reattach, but not to redevelop. At point 6 the flow is also reattaching. For point 11 the flow has no motion in y direction and shows the characteristics for fully developed duct flow.

Downstream from the second rib pair for the curve $x = 25\text{mm}$ the flow almost doesn't show any motion in the y -direction which indicates that the flow is probably reattached.

Analyzing the curve for $x = 5\text{mm}$ demonstrates that at point 1 a higher positive value in the y -direction due to flow separation at the second rib pair is present. Smaller velocities in the direction of the centerline are indicated at the points 8 and 9.

For the test volume between the two ribs just measurements for the points 17 and 18 (see Figure 6) were conducted due to limited access for the LDV and the noise associated with the walls. The points 18 and 19 pre assumed to be in the separation bubble. No exact predictions for these points can be made. For this region a finer grid would be desired since the flow motion is extremely complex. Figure 10, below, shows the measurements of the v -velocity fluctuation.

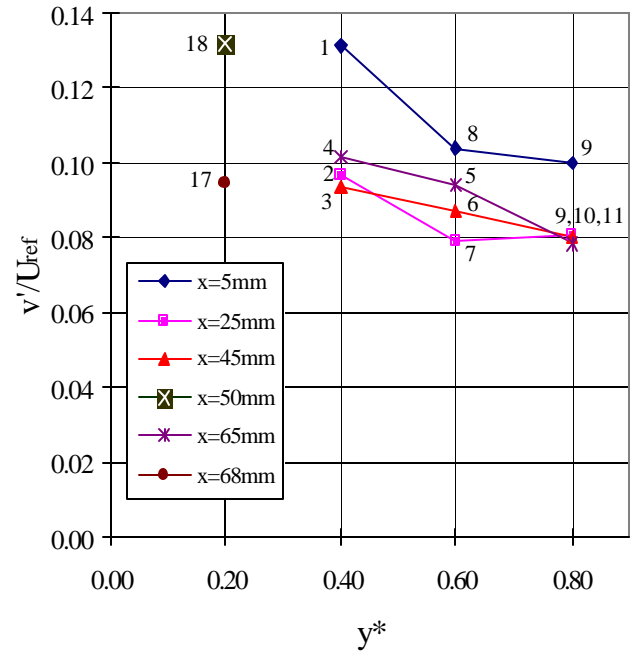


Figure 10 Fluctuation v -velocities in rough channel

CONCLUSIONS AND RECOMMENDATIONS

The LDV technique can be utilized to measure instantaneous velocities in roughened wall channel flow. This study has illustrated the technique's capability to non-intrusively measure the turbulence intensities in roughened wall duct flows. The experimental method produced high quality burst signals exemplified by the high power spectrum signal to noise ratios.

The turbulence intensities for rib-roughened walls were at a maximum near the height of the ribs rather than between the ribs. This is in contrast to smooth wall duct flows, where the turbulence intensity was a maximum near the wall. Greater nodal resolution is required to support this finding.

Greater spatial resolution will be required to quantitatively determine the effects of rib pitch and wall roughness. Although this study contributed to proof-of-experimental-concept and illustrated technique feasibility, additional spatial resolution will be required to utilize the results quantitatively. Small scale flow structures which may or may not occur over all Re numbers, near-wall measurement needs and closure modeling requirements dictate the need for many node points.

Accurate flow resolution between and near the rib surfaces requires direction detection for both velocity components. This is due to the difficulties associated with flow separation and reattachment. Although this study measured v -component direction sensitivity, the experimental apparatus to simultaneously determine the u -component direction was unavailable.

Differing LDV beam configurations will allow near wall measurements. Due to the angle of ingress, the standard beam configuration limits the measurement node wall proximity. A

skewed transmitter beam will allow for measurements very near to the surface structures such as walls, ribs, and corners.

ACKNOWLEDGMENTS

The majority of the work presented within is excerpted from Pantelic (1998). This work was performed under U.S. Department of Energy, Office of Basic Energy Sciences grant #DE-FG03-89ER14033 A002.

REFERENCES

Han, J. C., 1988, Heat Transfer and Friction Characteristics in Rectangular Channels with Rib Turbulators, *ASME Journal of Heat Transfer*, Vol. 110, 321-328.

Hwang, J. and Liou, T., 1994, Augmented Heat Transfer in a Rectangular Channel With Permeable Ribs Mounted on the Wall, *Journal of Heat Transfer*, Vol. 116, 912-920.

Hwang, J. and Liou, T., 1995, Heat Transfer and Friction in a Low-Aspect-Ratio Rectangular Channel With Staggered Perforated Ribs on Two Opposite Walls, *Journal of Heat Transfer*, Vol. 117, 843-850.

Liou, T., Chang, Y. and Hwang, D., 1990, Experimental and Computational Study of Turbulent Flows in a Channel With Two Pairs of Turbulence Promoters in Tandem, *Journal of Fluid Engineering*, Vol. 112, 302-310.

Liou, T., Wang, W. and Chang, Y., 1995, Holographic Interferometry Study of Spatially Periodic Heat Transfer in a Channel With Ribs Detached From One Wall, *Journal of Heat Transfer*, Vol. 117, 32-39.

Naimi, M. and Gessner, F. B., 1997, Calculation of Fully-Developed Turbulent Flow in Rectangular Ducts With Nonuniform Wall Roughness, *Journal of Fluid Engineering*, Vol. 119, 550-558.

Olsson, C. and Sunden, B., 1998, Experimental Study of Flow and Heat Transfer in Rib-Roughened Rectangular Channels, *Experimental Thermal and Fluid Science*, Vol. 16, 349-365.

Pantelic, D., 1998, Experimental Study of the Effects of Wall Roughness and the Free Stream Turbulent Energy Utilizing Laser Doppler Velocimetry Measurements, Diploma Thesis, Technische Universität München.

Rosen, C. and Tragardh, C., 1994, $\langle u'v' \rangle$ Reynolds Stress in the Viscous Sublayer over a Wide Range of Re Numbers, *AICHE Journal*, Vol. 40, No.1, 29-39.

Schlichting, H., 1960, "Boundary Layer Theory", McGraw-Hill Book Company, Inc., New York.

Travkin V. S. and Catton, I., 1992, Models of Turbulent Thermal Diffusivity and Transfer Coefficients for a Regular Packed Bed of Spheres, *Proc. 28th National Heat Transfer Conference, San Diego, CA, ASME, HTD-Vol. 193, 15-23.*

Travkin V. S. and Catton, I., 1995, A Two Temperature Model for Turbulent Flow and Heat Transfer in a Porous Layer, *Journal of Fluid Engineering*, Vol. 117, 181-188.

Zhang, Y. M., Gu, W. Z. and Han, J. C., 1994, Heat Transfer and Friction in Rectangular Channels With Ribbed or Ribbed - Grooved Walls, *Journal of Heat Transfer*, Vol. 116, 58-65.